Journal of Alloys and Compounds 513 (2012) 365–372

Contents lists available at SciVerse ScienceDirect

Journal of Alloys and Compounds

journal homepage: www.elsevier.com/locate/jallcom

Phase relations and Gibbs energies of spinel phases and solid solutions in the system Mg–Rh–O

K.T. Jacob[a,*], Debadutta Prusty[a], G.M. Kale[b]

[a] Department of Materials Engineering, Indian Institute of Science, Bangalore 560 012, India
[b] Institute for Materials Research, University of Leeds, Leeds, LS2 9JT, UK

ARTICLE INFO

Article history:
Received 26 August 2011
Received in revised form 14 October 2011
Accepted 18 October 2011
Available online 25 October 2011

Keywords:
Thermodynamic properties
Electromotive force (e.m.f.)
Free energy
Enthalpy
Entropy
Stability
Spinels
Solid solution
Phase diagram
Magnesium rhodite ($MgRh_2O_4$)
Magnesium rhodate (Mg_2RhO_4)

ABSTRACT

Pure stoichiometric $MgRh_2O_4$ could not be prepared by solid state reaction from an equimolar mixture of MgO and Rh_2O_3 in air. The spinel phase formed always contained excess of Mg and traces of Rh or Rh_2O_3. The spinel phase can be considered as a solid solution of Mg_2RhO_4 in $MgRh_2O_4$. The compositions of the spinel solid solution in equilibrium with different phases in the ternary system Mg–Rh–O were determined by electron probe microanalysis. The oxygen potential established by the equilibrium between $Rh + MgO + Mg_{1+x}Rh_{2-x}O_4$ was measured as a function of temperature using a solid-state cell incorporating yttria-stabilized zirconia as an electrolyte and pure oxygen at 0.1 MPa as the reference electrode. To avoid polarization of the working electrode during the measurements, an improved design of the cell with a buffer electrode was used. The standard Gibbs energies of formation of $MgRh_2O_4$ and Mg_2RhO_4 were deduced from the measured electromotive force (e.m.f.) by invoking a model for the spinel solid solution. The parameters of the model were optimized using the measured composition of the spinel solid solution in different phase fields and imposed oxygen partial pressures. The results can be summarized by the equations: $MgO + \beta\text{–}Rh_2O_3 \rightarrow MgRh_2O_4$; $\Delta G^\circ(\pm 1010)/J\,mol^{-1} = -32239 + 7.534T$; $2MgO + RhO_2 \rightarrow Mg_2RhO_4$; $\Delta G^\circ(\pm 1270)/J\,mol^{-1} = 36427 - 4.163T$; $\Delta G_M/J\,mol^{-1} = 2RT(x\,In\,x + (1-x)In(1-x)) + 4650x(1-x)$, where ΔG° is the standard Gibbs free energy change for the reaction and ΔG_M is the free energy of mixing of the spinel solid solution $Mg_{1+x}Rh_{2-x}O_4$.

1. Introduction

Rhodium metal and its oxides have many potential applications based on their chemical properties. The metal is used in automotive three-way catalysts for the oxidation of CO and hydrocarbons and reduction of NO_x present in exhaust gases [1,2]. Studies on Rh (1 1 1) [3] and Rh (1 0 0) [4] surfaces show that NO absorbs on rhodium at 100 K but dissociates into N_2 and O_2 on heating to 300 K. The major role of the catalyst in the oxidation of CO is to dissociate O_2 molecules, which occurs spontaneously in the adsorption process. The "free" oxygen atoms on the surface react with adsorbed CO to form CO_2 [5]. Gustafon et al. [5] have shown that a thin RhO_2 surface oxide film forms on metal Rh prior to the bulk Rh_2O_3 which has the corundum structure. Increase in CO_2 production has been correlated with the presence of thin RhO_2 surface film. Bulk Rh_2O_3 appears to poison the oxidation of CO. Further, anodic film formed on Rh electrode in an alkaline solution exhibits reversible color change between lemon yellow ($Rh_2O_3{\cdot}5H_2O$) and olive green ($RhO_2{\cdot}2H_2O$) on cycling applied potential [6]: an effect attributed to change in the oxidation state of metal ions. Rhodium detectors are used in nuclear reactors to measure neutron flux. Therefore, it is useful to study the stability of the different oxidation states of rhodium under various conditions.

Rhodium exists commonly in two valence states; Rh^{3+} and Rh^{4+}. The stable oxide phase in equilibrium with metallic Rh is Rh_2O_3, which has two polymorphic forms: α-Rh_2O_3 or the low-temperature form having corundum structure and β-Rh_2O_3 or the high-temperature form exhibiting orthorhombic structure. The oxidation of Rh always results in the formation of high temperature form of Rh_2O_3. In pure oxygen gas at ambient pressure β-Rh_2O_3 decomposes to metal at 1406 K, in air at 1315 K [7]. The corresponding temperatures for the decomposition of RhO_2 to β-Rh_2O_3 and oxygen are 1035 K and 955 K, respectively [8]. There is insufficient information on the stability of the two valence states in ternary and higher-order oxides. In general two ternary oxides, MRh_2O_4 with Rh in trivalent state and normal spinel structure and M_2RhO_4 with Rh in tetravalent state and inverse spinel structure, can exist in the systems M–Rh–O when ionic sizes are favorable. Since the two spinel phases can form a solid solution, Rh^{4+}

* Corresponding author. Tel.: +91 80 2293 2494; fax: +91 80 2360 0472.
E-mail addresses: katob@materials.iisc.ernet.in, ktjacob@hotmail.com (K.T. Jacob).

0925-8388/$ – see front matter © 2011 Elsevier B.V. All rights reserved.
doi:10.1016/j.jallcom.2011.10.050

ions can be stabilized in MRh_2O_4 even when pure inverse spinel M_2RhO_4 is unstable. Nell and O'Neill [9] have suggested that in the system Mg–Rh–O, the spinel $MgRh_2O_4$ contains significant concentration of Rh^{4+}. Thermodynamic properties and phase relations in Zn–Rh–O [10] and Cd–Rh–O [11] systems have been reported recently. But, the tetravalent state of rhodium appears to be absent in spinel phases belonging to these systems. The large band gap (~2.1 eV) of $ZnRh_2O_4$ and its transparency in the visible region suggest the absence of mixed valence states in this material [12]. Hence, the ternary system Mg–Rh–O was reinvestigated to confirm the stability of the tetravalent state of rhodium. The oxygen potential associated with three-phase equilibrium involving Rh, MgO and spinel "$MgRh_2O_4$" was measured in the temperature range from 975 to 1475 K. An advanced version of the solid-state cell incorporating a buffer electrode was used to eliminate errors caused by electrode polarization. The composition of the spinel phase "$MgRh_2O_4$" in equilibrium with (i) Rh and MgO, (ii) Rh and β-Rh_2O_3, (iii) MgO in air, and (iv) Rh in air were determined at different temperatures using electron probe microanalysis (EPMA) to accurately map the composition domain of the spinel phase. Gibbs free energy of formation of pure $MgRh_2O_4$ and Mg_2RhO_4 and free energy of mixing of the spinel solid solution are derived from the results. An isothermal section of phase diagram of the ternary system Mg–Rh–O and an oxygen potential diagram at 1373 K are composed from the results. Phase relations in air as a function of temperature are also computed.

2. Experimental methods

2.1. Materials

Attempts were made to synthesize stoichiometric $MgRh_2O_4$ by reacting an equimolar mixture of MgO and Rh_2O_3 in air at 1373 K for 60 ks, with intermediate regrinding and recompaction. The purity of the oxides used was greater than 99.99%. The oxides were dried at 973 K before use. The mixture was pressed into pellets at 100 MPa using a steel die. After reaction at high temperature, the pellets were quenched in liquid nitrogen. XRD analysis indicated the formation of a spinel phase, but with traces of residual Rh and Rh_2O_3. The lattice parameter of the cinnamon-colored spinel phase was 0.85174 nm. EPMA indicated that the spinel phase contained excess Mg compared to the stoichiometric composition. If the spinel phase is considered as a solid solution between $MgRh_2O_4$ and Mg_2RhO_4, the concentration of Mg_2RhO_4 can be evaluated as 4.4(±0.3) mole percent. Synthesis at 1273 K required longer times (~180 ks). The spinel phase was still nonstoichiometric, but with reduced amount of excess Mg. Trace of Rh_2O_3 was visible in SEM. Synthesis at lower temperatures was not attempted, because of the very lengthy heat treatment required for completion of reaction between the binary oxides. The nonstoichiometric spinel synthesized at 1373 K was used in electrochemical measurements and equilibrium studies described below.

2.2. Electrochemical measurements – cell assembly and procedure

The reversible e.m.f. of the solid-state electrochemical cell, Pt–13%Rh, Rh + MgO + "$MgRhO_4$"//$(Y_2O_3)ZrO_2$//O_2 (0.1 MPa), Pt–13%Rh was measured as a function of temperature over the range from 975 to 1475 K. The cell is written such that the right-hand electrode is positive. Impervious yttria-stabilized zirconia (YSZ) tube functioned as the solid electrolyte with predominant oxygen ion conduction (t_{ion} > 0.999) under the experimental conditions encountered in this study. Pure oxygen gas flowing at a pressure of 0.1 MPa served as the non-polarizable reference electrode. Working electrode of the cell consisted of a mixture of three condensed phases, metal Rh and two co-existing oxides MgO and "$MgRh_2O_4$". Because of trace hole (or electron) conductivity in the solid electrolyte, there is always a small electrochemical flux of oxygen from the electrode with high oxygen potential to the electrode having low oxygen potential. The flux is caused by coupled transport of oxygen ions and holes (or electrons) through the electrolyte. This flux can cause polarization of the working electrode, especially when they consist of three condensed phases. A buffer electrode, maintained at oxygen chemical potential close to that of the working electrode was introduced, as shown below, between reference and working electrodes to act as a sink for the electrochemical flux of oxygen and prevent the flux from reaching the working electrode. The oxygen flux from the reference electrode will take a lower resistance dissipation path by discharging into the buffer electrode rather than travel along the higher resistance (Y_2O_3) ZrO_2 bridge and through a second (Y_2O_3) ZrO_2 tube to reach the working electrode.

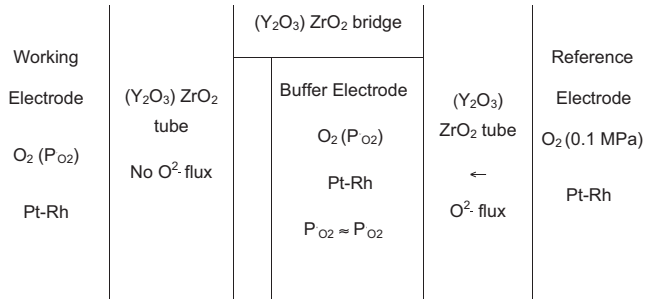

Thus, the three-electrode design of the cell prevents errors in the measured e.m.f. caused by polarization of the working electrode, ensuring accurate high-temperature thermodynamic measurements. The magnitude of the error caused by polarization in the conventional two electrode cell designs can be assessed from the difference in the e.m.f. between reference and buffer on the one hand, and reference and working electrodes on the other hand.

The cell design used for high-temperature e.m.f. measurements is shown in Fig. 1. It consisted of three distinct compartments, separated by impervious yttria-stabilized zirconia (YSZ) tubes and YSZ crucible. The working and reference electrodes were contained inside separate zirconia tubes. Construction of the high temperature galvanic cell was rendered more difficult by the introduction of the buffer electrode. Moreover, the partial pressure of oxygen at the working electrode was quite appreciable, especially at higher temperatures. Therefore, the static sealed design used by Charette and Flengas [13] was found more appropriate than other designs that employ either dynamic vacuum or inert gas flow over the electrodes.

Rhodium chloride solution was placed inside a close-end YSZ tube and heated gradually in argon gas to obtain a thin deposit of the metal on the inside surface of the tube. The thin deposit was converted to spherical particles by heat treatment at 1400 K. The working electrode was made by ramming an intimate mixture of three solid phases against the closed end of this YSZ tube with a short Rh lead wire embedded in the mixture. Rh, MgO and $MgRh_2O_4$ were taken in the molar ratio 1:1:1.5. The particle size of the powders used was in the range from 10 to 25 μm. The Rh lead was welded to a long Pt–13%Rh wire. An alumina sheath was used to insulate the metallic lead and to press the working electrode against the flat end of the zirconia tube. The top of the zirconia tube was closed with a tight-fitting bell-shaped pyrex tube, which supported a tungsten electrode connection sealed into the glass. The joint between the bell and the zirconia tube was sealed with the De Khotinsky cement. A spring placed between the bell and the alumina sheath applied pressure on the working electrode. The assembled working electrode half-cell was first evacuated using a side arm tube shown in the diagram, then the closed end of the YSZ tube was heated to ~600 K, and finally the connecting tube was flame sealed under vacuum. The working half-cell assembly rested on YSZ-stub contained in YSZ crucible, which provided the ionic bridge through the buffer electrode. As in the case of YSZ tube containing the working electrode, the inner surface of the crucible was also coated with Rh particles. The function of the coating is to minimize the interaction between MgO in the electrode mixture and YSZ tube. MgO has finite solubility in ZrO_2 and the dissolution process can have an effect on the e.m.f., albeit a minor one.

The buffer electrode was prepared by consolidating an intimate mixture of three solid phases in the YSZ crucible, with Rh lead embedded in the powder. Rh lead was connected to a long Pt–13%Rh wire. The three-phase mixture used in the buffer electrode was the same as that used in the working electrode, so that the oxygen potentials in the two electrodes are identical, at least at the start of the experiment at high temperature.

The inverted YSZ tube containing the reference electrode was first fixed inside the vertical quartz enclosure with De Khotinsky cement. The reference electrode was made by platinizing the inner surface of the tube and pressing a Pt mesh against the surface as shown in the diagram. Pt–13%Rh lead was spot welded to the Pt mesh. Pure oxygen gas at a pressure of 0.1 MPa was flowed through the inverted YSZ tube at a rate of 3 ml s^{-1}. The YSZ crucible containing the YSZ-stub was placed on top of the inverted tube. The working electrode assembly was then loaded into the crucible. The annular space between the zirconia tube and crucible was filled with the buffer electrode mixture. Finally, the top cover was cemented in place by melting the De Khotinsky cement in the ring container shown in Fig. 1. The top half of the cell assembly was identical to that developed by Charette and Flengas [13].

The entire assembly shown in Fig. 1 was placed inside a vertical resistance furnace, with the electrodes located in the even-temperature zone (±1 K). The joints between the Rh lead and Pt–13%Rh wire in the working and buffer electrodes and between Pt and Pt–13%Rh in the reference electrode were in the even temperature zone, so that there is no significant thermoelectric contribution to the e.m.f. The oxygen partial pressure in the evacuated and sealed enclosures around the working and buffer electrodes of the cell was established by the dissociation of "$MgRh_2O_4$" into Rh and MgO. The upper and lower parts of the assembly, where cement seals were located, remained at room temperatures during measurements. A Faraday cage made from thick stainless steel foil was placed between the furnace and the cell assembly. The foil was grounded to minimize induced e.m.f. on cell leads. The temperature of the furnace was controlled to ±1 K and was measured by a Pt/Pt–13%Rh

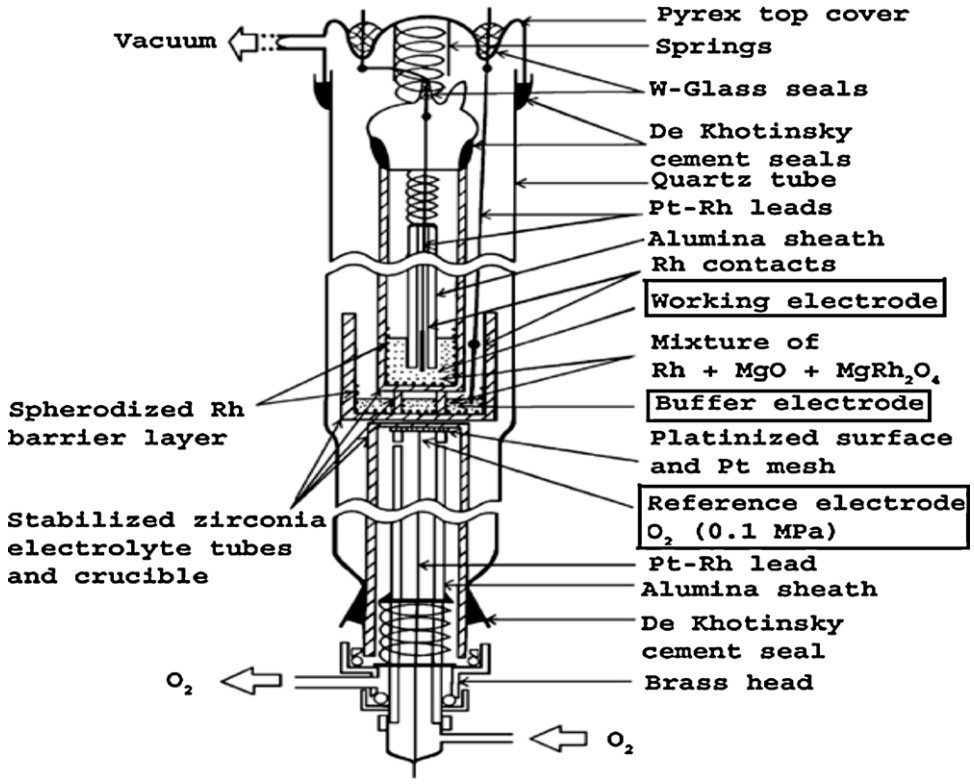

Fig. 1. Schematic diagram of the cell assembly used for electrochemical measurement.

thermocouple. The cell potentials were measured with a high-impedance digital voltmeter with a sensitivity of (±0.1) mV. The potential readings were corrected for small thermal e.m.f.s, measured separately using a symmetric cell with identical electrodes. At the end of each experiment, the electrodes were cooled to room temperature and examined using optical and scanning electron microscope and XRD. Although small changes in the relative concentration of the constituents were observed, the number and structure of the phases remained essentially unaltered.

2.3. Measurement of spinel composition

The compositions of the spinel phase in equilibrium with (i) Rh and MgO, (ii) Rh and β-Rh_2O_3, (iii) MgO in air, and (iv) Rh in air, at different temperatures, were measured using EPMA. Pelletized three-phase mixture of Rh + MgO + $MgRh_2O_4$ contained in MgO crucible was placed in quartz tube, which was evacuated to 1 Pa and sealed under vacuum. The oxygen partial pressure inside the ampoules was established by the dissociation of $MgRh_2O_4$ to Rh and MgO. Similarly, the three-phase mixture Rh + β-Rh_2O_3 + $MgRh_2O_4$ wrapped in Rh foil was equilibrated in an evacuated quartz ampoule. The oxygen partial pressure in this case is controlled by the dissociation of Rh_2O_3 to Rh. Two-phase mixtures of MgO + $MgRh_2O_4$ contained in an MgO crucible and Rh + $MgRh_2O_4$ wrapped in Rh foil were equilibrated in dry synthetic air. The mixtures were equilibrated for ~45 ks at 1173 K and ~30 ks at 1373 K. Longer heat treatment did not alter the composition of the spinel solid solution. After equilibration the samples were quenched in liquid nitrogen.

3. Results and analysis

The reversible e.m.f. of the solid-state electrochemical cell is shown in Fig. 2 as a function of temperature in the range from 975 K to 1475 K. The e.m.f. decreases linearly with increasing temperature. The least-squares regression analysis gives the following expression:

$$E(\pm 1.72)/mV = 734.94 - 0.4945T \quad (1)$$

The uncertainty limit corresponds to twice the standard deviation (2σ). The e.m.f. between reference and buffer electrode was lower than the e.m.f. between reference and working electrode by 1–11 mV because of the polarization of the buffer electrode: polarization loss is higher at lower temperatures. The open circuit potential of the solid-state cell is related to the ratio of oxygen partial pressures at the two electrodes:

$$E = \frac{RT}{4F} \ln\left(\frac{P^0_{O_2}}{P_{O_2}}\right) \quad (2)$$

where P_{O_2} and $P^0_{O_2}$ are the oxygen pressures at the working and reference electrodes respectively, F is the Faraday constant, and R the gas constant. As pure oxygen at 0.1 MPa was used as the reference electrode, the oxygen potential ($\Delta\mu_{O_2} = RT \ln P_{O_2}$) corresponding to the three-phase equilibrium involving Rh, MgO and

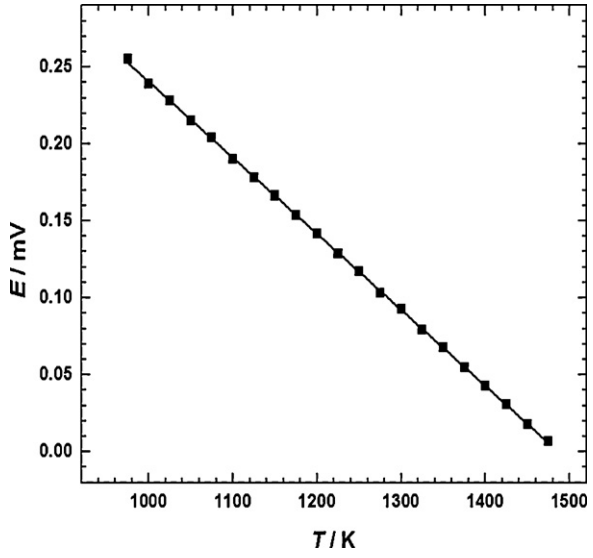

Fig. 2. Variation of the e.m.f. of the cell with temperature.

Table 1
Composition of the spinel solid solution $Mg_{1+x}Rh_{2-x}O_4$ in various phase fields of the system Mg–Rh–O.

T (K)	Composition of spinel solid solution, mol% Mg_2RhO_4 in $MgRh_2O_4$ (100x)			
	Phase fields			
	MgO + Rh + Spinel s.s.	Rh + Rh_2O_3 + Spinel s.s.	MgO + Spinel s.s. ($P_{O_2}/P^o = 0.21$)	Rh + Spinel s.s. ($P_{O_2}/P^o = 0.21$)
1173	3	0.6	5.4	
1373	5.8	1.6	6.1	4.3
1473	7.5			

the spinel phase at the working electrode, is directly related to the e.m.f.:

$$\Delta\mu_{O_2}(\pm 665)/\mathrm{J\ mol^{-1}} = -4FE = -283643 + 190.85T \quad (3)$$

The compositions of the spinel phase, in equilibrium with (i) Rh and MgO, (ii) Rh and β-Rh_2O_3, (iii) MgO in air, (iv) Rh in air, at different temperatures measured using EPMA are summarized in Table 1. The average uncertainty in composition is 0.3 mol%. It is seen that pure $MgRh_2O_4$ does not exist in equilibrium with Rh and MgO. The "$MgRh_2O_4$" phase has a small amount of dissolved Mg_2RhO_4 forming a spinel solid solution. The concentration of tetravalent rhodium ions in the spinel solid solution increases with temperature. The measured oxygen potential corresponding to three-phase equilibrium is therefore defined by two independent reactions that define the composition of the solid solution. The reactions are:

$$\mathrm{MgO} + 2\mathrm{Rh}(s) + \frac{3}{2}\mathrm{O_2} \rightarrow \mathrm{MgRh_2O_4} \quad (4)$$

$$\Delta G_4^o = 1.5\Delta\mu_{O_2} - RT\ln a_{MgRh_2O_4} \quad (5)$$

$$2\mathrm{MgO} + \mathrm{Rh}(s) + \mathrm{O_2} \rightarrow \mathrm{Mg_2RhO_4} \quad (6)$$

$$\Delta G_6^o = \Delta\mu_{O_2} - RT\ln a_{Mg_2RhO_4} \quad (7)$$

$MgRh_2O_4$ has a normal spinel structure with Mg^{2+} ion on tetrahedral site and two Rh^{3+} ions on octahedral site. Although normal spinels show partial disorder with increase in temperature, the large octahedral site preference energy of Rh^{3+} probably minimizes cation disorder in $MgRh_2O_4$. The octahedral splitting of d orbital in Rh^{3+} leads to fully occupied t_{2g}^6 (low spin state) and empty e_g^o states. In the inverse spinel Mg_2RhO_4, half of Mg cations occupy tetrahedral sites and the remaining Mg cations and all the Rh^{4+} ions are distributed on octahedral sites. When the two spinel compounds are mixed, the mixing of Mg^{2+}, Rh^{3+} and Rh^{4+} occur on octahedral sites. Assuming that the mixing of cations is ideal (Temkin model), the activity of each component is the square of its mole fraction:

$$a_{MgRh_2O_4} = X^2_{MgRh_2O_4} = (1 - X_{Mg_2RhO_4})^2 = (1-x)^2 \quad (8)$$

$$a_{Mg_2RhO_4} = X^2_{Mg_2RhO_4} = x^2 \quad (9)$$

where $x = X_{Mg_2RhO_4}$ represents the mole fraction of Mg_2RhO_4. Using the ideal mixing model and the measured composition of the spinel solid solution corresponding to three-phase equilibrium, an estimate of the standard Gibbs energy changes corresponding to reactions (4) and (6) is obtained at three temperatures, 1173, 1373 and 1473 K, as shown in Figs. 3 and 4. It is seen that the activity contribution is small relative to the measured oxygen potential for $MgRh_2O_4$ since the spinel solid solution in equilibrium with Rh and MgO is rich in this component. The activity correction is large for Mg_2RhO_4 because it is a minor component of the spinel solid solution. Linear equations connecting these points are then developed for the Gibbs energy of formation of the two pure spinel phases. Using these equations, five compositions of the spinel phase in equilibrium with (i) Rh and β-Rh_2O_3, (ii) MgO in air, and (iii) Rh in air are calculated. However, they do not agree well with values obtained from EPMA (Table 1). To improve the fit to experimental

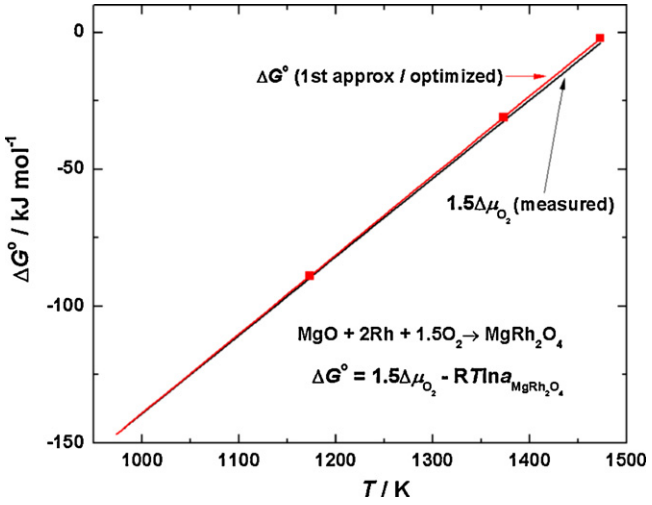

Fig. 3. Standard Gibbs free energy of formation of $MgRh_2O_4$ from MgO, Rh and O_2 with and without correction for the activity of $MgRh_2O_4$.

data, the model for the spinel solid solution is modified by adding a term for enthalpy of mixing:

$$\Delta H_M = \Delta G_M^E = \Omega.X_{Mg_2RhO_4}\cdot(1 - X_{Mg_2RhO_4}) = \Omega.x.(1-x) \quad (10)$$

where Ω denotes the regular solution parameter. The activities of $MgRh_2O_4$ and Mg_2RhO_4 are now equal to the product of the square

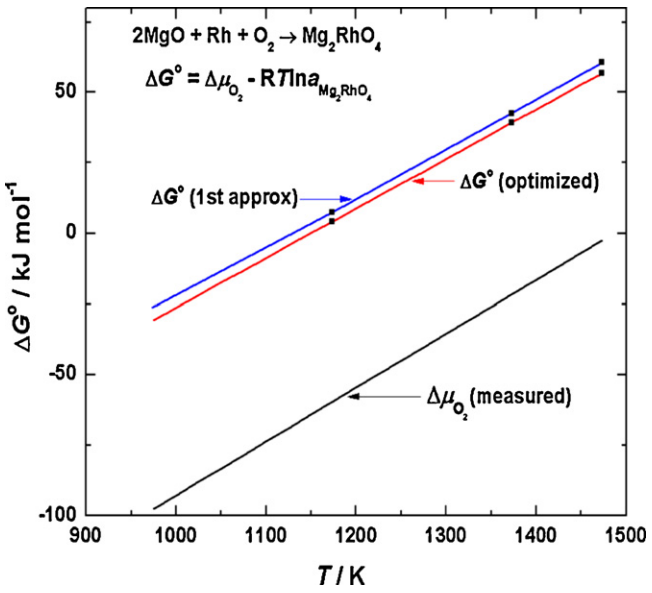

Fig. 4. Gibbs energy of formation of Mg_2RhO_4 from MgO, Rh and O_2 using different models for the spinel solid solution.

of their mole fractions and the corresponding activity coefficients (γ_i) defined by:

$$RT \ln \gamma_{MgRh_2O_4} = \Omega . X^2_{Mg_2RhO_4} = \Omega . x^2 \quad (11)$$

$$RT \ln \gamma_{Mg_2RhO_4} = \Omega . (1 - X_{Mg_2RhO_4})^2 = \Omega . (1 - x)^2 \quad (12)$$

In the regular solution model with ideal Temkin mixing, the activities in the spinel solid solution are defined by:

$$\ln a_{MgRh_2O_4} = \frac{\Omega}{RT} X^2_{Mg_2RhO_4} + 2\ln(1 - X_{Mg_2RhO_4}) = \frac{\Omega}{RT} x^2 + 2\ln(1 - x) \quad (13)$$

$$\ln a_{Mg_2RhO_4} = \frac{\Omega}{RT} (1 - X_{Mg_2RhO_4})^2 + 2\ln X_{Mg_2RhO_4} = \frac{\Omega}{RT} (1 - x)^2 + 2\ln x \quad (14)$$

Using initially an arbitrary estimate for Ω, the standard Gibbs energies of formation of the pure spinel compounds and the compositions of the solid solution in different phase field defined in Table 1 are calculated. The value of Ω is then changed in steps till the calculated compositions matched the experimental data. The value of Ω giving a good fit to experimental data obtained by successive iterations is 4650 J mol^{-1}. The ionic radii of Mg^{2+}, Rh^{3+} and Rh^{4+} for six-fold coordination are 0.072, 0.065 and 0.060 nm, respectively [14]. Therefore, replacement of Rh^{3+} ion on the octahedral site of the normal spinel $MgRh_2O_4$ by Mg^{2+} and Rh^{4+} from the inverse spinel Mg_2RhO_4 can introduce local strains in the structure and result in positive enthalpy of mixing. Since the average ionic radius of the substituting ions Mg^{2+} and Rh^{4+} (0.066 nm) is close to that of Rh^{3+} (0.065 nm), the magnitude of the enthalpy of mixing is likely to be relatively small.

Using the optimized value of the regular solution parameter, Ω, the improved values for the standard Gibbs energy of formation of $MgRh_2O_4$ and Mg_2RhO_4 according to Eqs. (4) and (6) are obtained at two temperatures. These are plotted in Figs. 3 and 4 respectively. For $MgRh_2O_4$, incorporation of the enthalpy of mixing in the model for the solid solution does not significantly change the derived value for Gibbs energy of formation, because the composition of the solid solution is close to that of the pure compound. On the contrary, in case of Mg_2RhO_4 there is a significant difference between the data calculated using the ideal Temkin model and the revised regular solution model, since this component is present as a solute at low concentration in the spinel solid solution. The refined values for the standard Gibbs energy of formation of pure spinel compounds from MgO, Rh and O_2 can be represented by the equations;

$$\Delta G^o_4(\pm 1000)/\text{J mol}^{-1} = -428604 + 289.534T \quad (15)$$

$$\Delta G^o_6(\pm 900)/\text{J mol}^{-1} = -201991 + 175.72T \quad (16)$$

Based on the revised regular solution model and ideal Temkin entropy of mixing, the free energy of mixing of the spinel solid solution $Mg_{1+x}Rh_{2-x}O_4$, ΔG_M, is given by:

$$\Delta G_M/\text{J mol}^{-1} = 2RT(x\ln x + (1-x)\ln(1-x)) + 4650x(1-x) \quad (17)$$

4. Discussion

4.1. Three-phase equilibrium – comparison with data in the literature

The oxygen chemical potential corresponding to three-phase equilibrium involving Rh + MgO + $MgRh_2O_4$ obtained in this study is compared with data reported by Nell and O'Neill [9] in Fig. 5 as a function of temperature. While there is good agreement at the higher temperatures, there is significant deviation at the lower temperatures: the oxygen potential measured in this study is more negative by 3.84 kJ mol^{-1} at 975 K. This would imply that the e.m.f. measured by Nell and O'Neill [9] using air as the reference electrode is lower by ~10 mV at this temperature. The magnitude of the polarization loss detected in this study is of the same order, suggesting that polarization of the three-phase electrode used by Nell and O'Neill [9] may be the reason for the difference. While both studies confirm that the spinel phase has significant concentration of Rh^{4+} ions, the concentration of the spinel phase at 1373 K measured in the two studies show some difference. For example, the concentration of Mg_2RhO_4 in $MgRh_2O_4$ reported by Nell and O'Neill [9] is 8 mol%, where as the corresponding composition obtained in this study is 5.8 (±0.3) mol% for three-phase equilibrium.

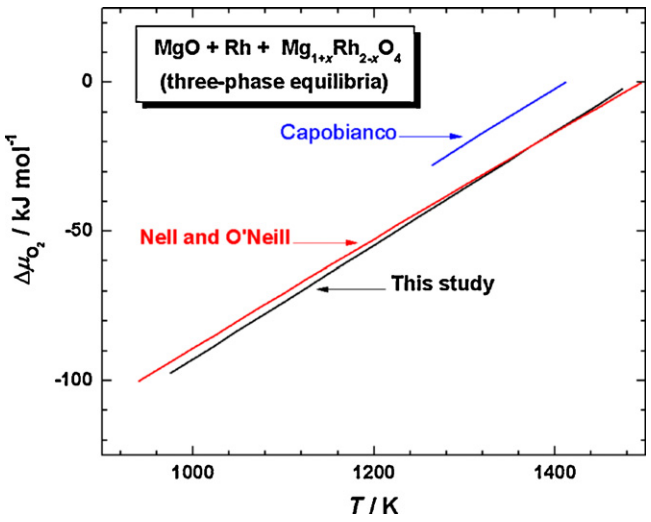

Fig. 5. Comparison of oxygen potential for the three-phase equilibrium, involving MgO, Rh and $Mg_{1+x}Rh_{2-x}O_4$, obtained in this study with data reported by Nell and O'Neill [9] and Capobianco [15].

Capobianco [15] measured the decomposition temperature of $MgRh_2O_4$ in oxygen, air and an oxygen-nitrogen gas mixture containing 7% oxygen by observing the formation of Rh crystals on the surface of $MgRh_2O_4$. Although there was no evidence of MgO on the surface, Capobianco [15] assumed that the spinel decomposed according to reaction (4). The oxygen potentials reported by Capobianco [15] are significantly more positive than those obtained in this study. The temperature dependence of the oxygen potential is also significantly different. It is probable that the values of Capobianco [15] do not pertain to the equilibrium between three condensed phases, but to one involving two phases, Rh and spinel solid solution. This two-phase boundary will be computed in a subsequent section on phase diagrams.

4.2. Gibbs energy of formation of pure spinel compounds from component binary oxides

The standard Gibbs free energy of formation of β-Rh_2O_3 ($\Delta G^o_f(\beta - Rh_2O_3)$) measured by Jacob and Sriram [7] can be represented by the equations:

$$2Rh + \frac{3}{2}O_2 \rightarrow \beta - Rh_2O_3 \quad (18)$$

$$\Delta G^o_f(\beta - Rh_2O_3)(\pm 120)/\text{J mol}^{-1} = -396365 + 282.0T \quad (19)$$

Coupling Eqs. (15) and (19), the Gibbs energy of formation of $MgRh_2O_4$ from MgO and β-Rh_2O_3 (ΔG^{o}_{20}) is obtained. For the reaction,

$$MgO + \beta\text{-}Rh_2O_3 \rightarrow MgRh_2O_4 \quad (20)$$

$$\Delta G^{o}_{20}(\pm 1010)/\text{J mol}^{-1} = -32239 + 7.534T \quad (21)$$

The standard Gibbs free energy of formation of RhO_2 ($\Delta G^{o}_{f}(RhO_2)$) according to the reaction,

$$Rh + O_2 \rightarrow RhO_2 \quad (22)$$

obtained from recent measurements [8] can be represented by the equation;

$$\Delta G^{o}_{f}(RhO_2)(\pm 71)/\text{J mol}^{-1} = -238,418 + 179.89T \quad (23)$$

Combining Eq. (16) and (23), the Gibbs energy of formation of Mg_2RhO_4 (ΔG^{o}_{24}) from its component binary oxides,

$$2MgO + RhO_2 \rightarrow Mg_2RhO_4 \quad (24)$$

is obtained as:

$$\Delta G^{o}_{24}(\pm 1270)/\text{J mol}^{-1} = 36427 - 4.163T \quad (25)$$

The second-law enthalpy of formation of the 2–3 spinel $MgRh_2O_4$ from its component oxides MgO and β-Rh_2O_3 at a mean temperature of 1225 K is negative (-32.24 ± 0.93 kJ mol^{-1}), whereas the corresponding value for the 2–4 spinel Mg_2RhO_4 from MgO and RhO_2 is positive (36.43 ± 4 kJ mol^{-1}). Thus, Mg_2RhO_4 is unstable relative to its component binary oxides. Despite the instability of Mg_2RhO_4, Rh^{4+} ions are present because the unstable compound can be stabilized as a dilute solution in another stable compound ($MgRh_2O_4$) with the same structure.

The second-law entropy of formation of $MgRh_2O_4$ from its component oxides is −7.53 (±0.76) J mol^{-1} K^{-1}. The corresponding value for Mg_2RhO_4 is positive (4.16 ± 3.3 J mol^{-1} K^{-1}). The difference of 11.69 J mol^{-1} K^{-1} is fortuitously close to the configuration entropy of the inverse spinel (11.53 J mol^{-1} K^{-1}) arising from the mixing of two ions $Mg^{2+}$and Rh^{4+} on the octahedral site.

Although heat capacity of data for $MgRh_2O_4$ has been measured from 360 to 1065 K [9], the data probably corresponds to a spinel solid solution containing some Rh^{4+} ions. Combining the heat capacity data for $MgRh_2O_4$ [9] with those for Rh_2O_3 [16] and MgO [17], it is possible to calculate enthalpy of formation and entropy of $MgRh_2O_4$ at 289.15 K. The enthalpy of formation of $MgRh_2O_4$ from its component binary oxides at 298.15 K thus obtained is −35.51 (±2.2) kJ mol^{-1}. The standard entropy of $MgRh_2O_4$ at the same temperature is 89.05 (±3.1) J mol^{-1} K^{-1}. The standard entropies of Rh_2O_3 from reference [16] and MgO from [17] are used in the calculation.

In view of the uncertainty in the composition of $MgRh_2O_4$ used for C_P measurement, it is probably safer to estimate the properties at 298.15 K using the Neumann–Kopp rule. In this scenario, enthalpy of formation from component oxides is −32.24 (±2) kJ mol^{-1}. The standard enthalpy of formation of $MgRh_2O_4$ from its elements at 298.15 K is −1039.26 (±4) kJ mol^{-1}. The standard entropy of $MgRh_2O_4$ at 298.15 K becomes 95.1 (±3.5) J mol^{-1} K^{-1}. Auxiliary data for Rh_2O_3 from reference [16] and MgO from [17] are used in this calculation.

Recent studies indicate that unlike $MgRh_2O_4$, $CdRh_2O_4$ [11] and $ZnRh_2O_4$ [10] are stoichiometric. A small solubility of the inverse 2–4 spinel Mg_2RhO_4 in the normal 2–3 spinel $MgRh_2O_4$ is the main reason for the small composition range exhibited by $MgRh_2O_4$. The reason for the greater prominence of Rh^{4+} ion in $MgRh_2O_4$ compared to $CdRh_2O_4$ [11] and $ZnRh_2O_4$ [10] may reside in the greater tetrahedral site preference of Cd and Zn compared to Mg. The 2–4 (M_2RhO_4) spinel compounds of Cd and Zn containing Rh in tetravalent state would be more unstable than the corresponding compound of Mg because of the one divalent ion has to occupy the octahedral site in the inverse spinel. Pushing Cd and Zn into octahedral sites is energetically unfavorable. Since Mg has octahedral preference, the Mg 2–4 spinel would be relatively more stable. For a given divalent ion (M), the more unstable the 2–4 spinel, the lower would be the concentration of Rh^{4+} in the corresponding 2–3 spinel (MRh_2O_4). Extending this logic and excluding the effect of other factors, one would expect more Rh^{4+} in 2–3 spinel compounds with divalent ions such as Ni^{2+} having octahedral site preference. This hypothesis needs to be tested by experiment.

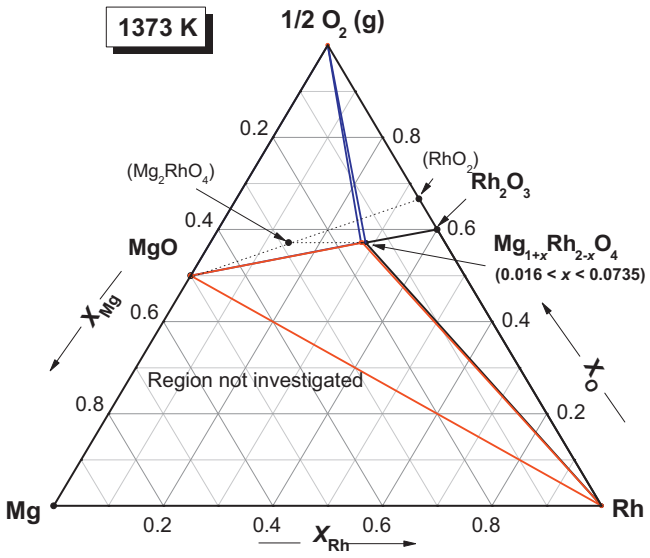

Fig. 6. Isothermal section of the phase diagram for the system Mg–Rh–O at 1373 K.

4.3. Construction of phase diagrams

An isothermal section of the phase diagram for the system Mg–Rh–O at 1373 K constructed from the results of this study is shown in Fig. 6. Along the binary Mg–O, only one oxide MgO is present. Similarly, along the Rh–O boundary, β-Rh_2O_3 with orthorhombic structure is the only stable compound. The binary phase diagram Mg–Rh is not well established and no experiments were conducted in this study in phase fields involving the alloy phase. Although two ternary compounds $MgRh_2O_4$ and Mg_2RhO_4 can exist in the Mg–Rh–O ternary, the only stable phase is $MgRh_2O_4$. However, the phase does not appear on the phase diagram as a pure phase. It contains small amount of Mg_2RhO_4 in solid solution, which can be represented as $Mg_{1+x}Rh_{2-x}O_4$ ($0.016 < x < 0.0735$). Two three-phase fields involving MgO + Rh + spinel s.s. and Rh + Rh_2O_3 + spinel s.s. are identified. Narrow two-phase fields identified are Rh + spinel s.s. and O_2 + spinel s.s.

An oxygen potential diagram for the system Mg–Rh–O at 1373 K, computed from the results obtained in this study, is shown in Fig. 7. The experimentally determined compositions are also displayed for comparison. The composition of phases is represented by cationic fraction, $\eta_{Rh}/(\eta_{Rh} + \eta_{Mg})$, where η_i denotes the number of moles of component i. Since oxygen is not included in the composition parameter, information on oxygen nonstoichiometry cannot be displayed on the diagram. Nevertheless, the diagram provides useful information on the oxygen potential range for the stability of various phases. The diagram is complementary to the Gibbs triangle representation of phase relations in a ternary system (Fig. 6) where phase compositions are unambiguously displayed. All the topological rules of construction for conventional temperature-composition phase diagrams are applicable to the oxygen potential diagram shown in Fig. 7.

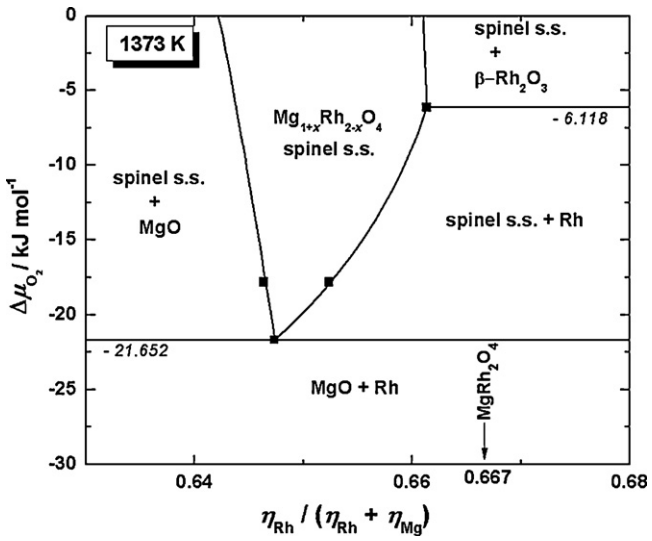

Fig. 7. Isothermal oxygen potential diagram for the system Mg–Rh–O at 1373 K calculated using results obtained in this study. The compositions determined in this study are indicated by points (■).

When three condensed phases are at equilibrium with a gas phase in a ternary such as Mg–Rh–O, the system is monovariant; at a fixed temperature the three condensed phases coexist only at a unique partial pressure of oxygen. Therefore, horizontal lines on the diagram represent three-phase equilibrium. The figure shows that at an oxygen potential below −21.652 kJ mol^{-1}, the spinel solid solution ($Mg_{1+x}Rh_{2-x}O_4$) decomposes to MgO and Rh.

When the spinel solid solution is in equilibrium with MgO and Rh, the composition of the solid solution is simultaneously defined by Eqs. (4) and (6). Substituting activity values in Eqs. (5) and (7) the composition of spinel solid solution in equilibrium with MgO and Rh can be calculated at different temperatures. The calculated values are summarized in Table 2. With decrease in temperature, the composition shifts towards the stoichiometric value. The calculated values agree very well with experimental data for three temperatures. This is expected since the value of the regular solution parameter Ω was derived from these compositions.

The two-phase equilibrium between spinel solid solution and MgO is governed by the reaction:

$$MgRh_2O_4 + 3MgO + \frac{1}{2}O_2 \rightarrow 2Mg_2RhO_4 \quad (26)$$

$$\Delta G^{o}_{26}(\pm 2060)/\text{J mol}^{-1} = 24622 + 61.92T \quad (27)$$

where ΔG^{o}_{26} is obtained by combining Eqs. (15) and (16). The two-phase boundary in the diagram was obtained by calculating the values of X_{MgRhO_4} that satisfy the above equation at several oxygen partial pressures. Similarly, the equation representing the two-phase equilibrium between spinel solid solution and Rh is:

$$Mg_2RhO_4 + 3Rh + 2O_2 \rightarrow 2MgRh_2O_4 \quad (28)$$

$$\Delta G^{o}_{28}(\pm 2195)/\text{J mol}^{-1} = -655217 + 403.34T \quad (29)$$

Table 2
Computed composition of the spinel solid solution corresponding to three-phase equilibrium between Rh, MgO and $Mg_{1+x}Rh_{2-x}O_4$ expressed as cationic fraction.

T (K)	Composition of spinel solid solution $\eta_{Rh}/(\eta_{Rh}+\eta_{Mg})$
973	0.6627
1173	0.6567
1373	0.6473
1473	0.6418

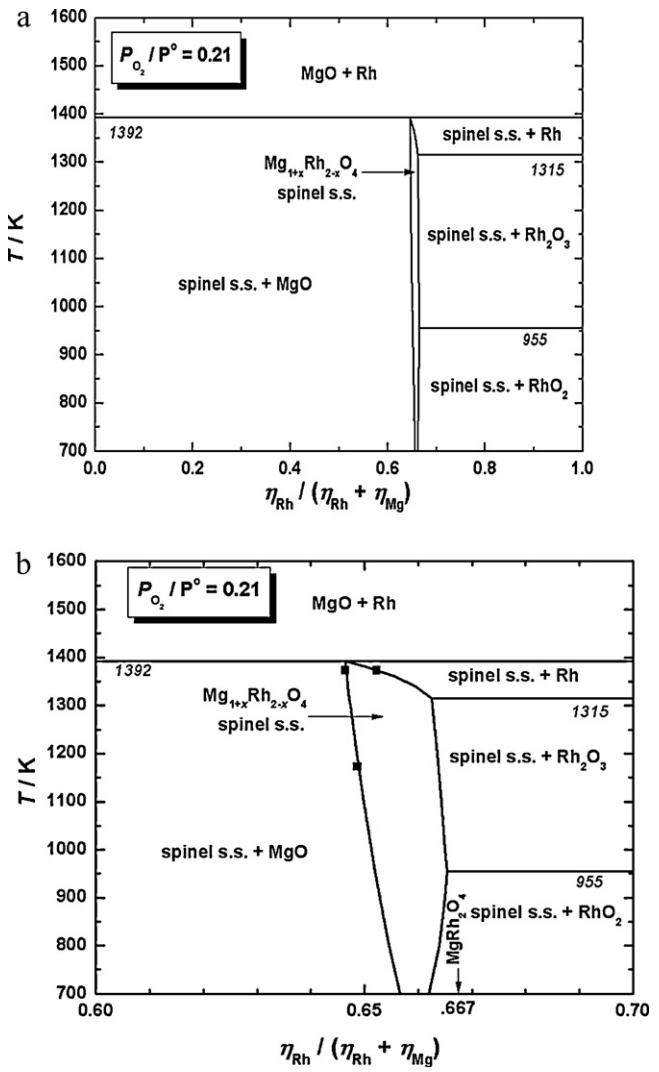

Fig. 8. (a) Computed phase relations in the system Mg–Rh–O as a function of temperature in air. (b) Enlarged view of the spinel single phase region in air as a function of temperature. The compositions determined in this study are indicated by points (■).

The measurements of Capobianco [15] probably lie along this boundary of the spinel stability. The two-phase boundary between spinel and Rh_2O_3 can be computed using the equation:

$$Mg_2RhO_4 + \frac{3}{2}Rh_2O_3 \rightarrow 2MgRh_2O_4 + \frac{1}{4}O_2 \quad (30)$$

$$\Delta G^{o}_{30}(\pm 2210)/\text{J mol}^{-1} = -60669.5 - 19.66T \quad (31)$$

Equilibria at very low oxygen potentials between alloys and oxides are not shown, since thermodynamic properties of Mg–Rh alloys required for the calculation are not available in the literature. Oxygen potential diagrams at other temperatures can be readily computed from the thermodynamic data if required for a specific application.

Phase relations can also be calculated as a function of temperature at constant oxygen partial pressures. The computed phase diagram in air ($P_{O_2}/P^o = 0.21$) is shown in Fig. 8(a) for the entire range of composition. An expanded view of the spinel phase field is given in Fig. 8(b) together with experimental data obtained in this study. The calculated decomposition temperature of the spinel solid solution in air is 1392 (±1.2) K, which is in good accord with the value of 1393 (±5) K reported by Skrobot and Grebenshchikov [18]. This value is also close to the temperature

1393 (±1.5) K calculated from the oxygen potential data measured by Nell and O'Neill [9] for $MgRh_2O_4$. Thus, the decomposition temperature of the spinel phase in air is in very good agreement between the three studies. The decomposition temperature in pure oxygen at 0.1 MPa pressure computed from the results of this study is 1486 (±1.2) K. It is clear from Fig. 8(b) that pure spinel compound $MgRh_2O_4$ cannot be made from component oxides in air. The closest approach of the spinel composition to stoichiometry occurs at 955 K, a temperature too low for solid state synthesis.

5. Conclusions

Experimental measurement of the composition of the spinel phase in different phase fields and oxygen partial pressures using an electron microprobe indicates that pure $MgRh_2O_4$ does not exist at high temperatures. There is some solubility of Mg_2RhO_4 in $MgRh_2O_4$. An advanced design of the solid-state cell incorporating a buffer electrode is used for the precise measurement of oxygen potential corresponding to the three-phase field involving Rh, MgO and spinel solid solution. A regular solution model based on ideal mixing of ions on the octahedral site is used to describe the activities of the spinel components in the solid solution. The parameters of this model are optimized by using experimental values of compositions of spinel solid solution in different phase fields and imposed oxygen partial pressures. A unique method of analysis of e.m.f. of a solid state cell to derive thermodynamic properties of two compounds ($MgRh_2O_4$ and Mg_2RhO_4) that form a solid solution is presented.

The Gibbs energies of formation of $MgRh_2O_4$ and Mg_2RhO_4 from their component binary oxides are evaluated from the results of this study and information on binary oxides available in the literature. For the reaction, $MgO + \beta\text{-}Rh_2O_3 \rightarrow MgRh_2O_4$, ΔG° $(\pm 1010)/\mathrm{J\,mol^{-1}} = -32239 + 7.534T$; for $2MgO + RhO_2 \rightarrow Mg_2RhO_4$, ΔG° $(\pm 1270)/\mathrm{J\,mol^{-1}} = 36427 - 4.163T$. The free energy of mixing of the spinel solid solution is defined by: $\Delta G_M/\mathrm{J\,mol^{-1}} = 2RT\,(x \ln x + (1-x) \ln (1-x)) + 4650\,x\,(1-x)$, where x is the mole fraction of Mg_2RhO_4. Based on the thermodynamic data obtained in this study, phase relations are computed and displayed graphically as a function of oxygen potential at fixed temperature, and as a function of temperature at constant oxygen partial pressure. The results of this study indicate that ternary oxides with all rhodium ions in tetravalent state may not be stable at high temperatures and ambient pressure. Nevertheless, when such oxides can form a solid solution with another phase in which rhodium in trivalent, then mixed valence phases are obtained. Clearly identified are factors that stabilize tetravalent rhodium in the ternary oxide phase in the system Mg–Rh–O. The new understanding can be used to design complex oxide phases that contain tetravalent rhodium at high temperatures.

Acknowledgements

K.T. Jacob wishes to thank the Indian National Academy of Engineering, New Delhi, for support as INAE Distinguished Professor. D. Prusty is grateful to the Indian Academy of Sciences, Bangalore, for the award of summer research fellowship at the Indian Institute of Science.

References

[1] K.C. Taylor, Catal. Rev. Sci. Eng. 35 (1993) 457–481.
[2] M. Schelef, G.W. Graham, Catal. Rev. Sci. Eng. 36 (1994) 433–457.
[3] H.J. Borg, J.F.C.-J.M. Reijerse, R.A. van Santen, J.W. Niemantsverdriet, J. Chem. Phys. 101 (1994) 10052–10063.
[4] P. Ho, J.M. White, Surf. Sci. 137 (1984) 103–116.
[5] J. Gustafon, R. Westerström, A. Resta, A. Mikkelsen, J.N. Andersen, O. Balmes, X. Torrelles, M. Schmid, P. Varga, B. Hammer, G. Kresse, C.J. Baddeley, E. Lundgren, Catal. Today 145 (2009) 227–235.
[6] H. Wang, M. Yan, Z. Jiang, Thin Solid Films 401 (2001) 211–215.
[7] K.T. Jacob, M.V. Sriram, Metall. Mater. Trans. A 25A (1994) 1347–1357.
[8] K.T. Jacob, D. Prusty, J. Alloys Compd. 507 (2010) L17–L20.
[9] J. Nell, H.S.C. O'Neill, Geochim. Cosmochim. Acta 61 (1997) 4159–4171.
[10] A. Banerjee, Z. Singh, J. Solid State Electrochem. 13 (2009) 1201–1207.
[11] A. Banerjee, Z. Singh, V. Venugopal, Solid State Ionics 180 (2009) 1337–1341.
[12] H. Ohta, K. Nomura, H. Hiramatsu, K. Ueda, T. Kamiya, M. Hirano, H. Hosono, Solid-State Electron. 47 (2003) 2261–2267.
[13] G.G. Charette, S.N. Flengas, J. Electrochem. Soc. 115 (1968) 796–804.
[14] R.D. Shannon, Acta Crystallogr. A 32 (1976) 751–767.
[15] C.J. Capobianco, Thermochim. Acta 220 (1993) 7–16.
[16] K.T. Jacob, T. Uda, T.H. Okabe, Y. Waseda, High Temp. Mater. Process 19 (2000) 11–16.
[17] L.B. Pankratz, Thermodynamic Properties of Elements and Oxides, Bulletin 672, United States Department of the Interior, Bureau of Mines, 1982, p. 227.
[18] V.N. Skrobot, R.G. Grebenshchikov, Zh. Neorg. Khim. 42 (1997) 1751–1754.